
MORPHSEEK: FINE-GRAINED LATENT REPRESENTATION-LEVEL POLICY OPTIMIZATION FOR DEFORMABLE IMAGE REGISTRATION

A PREPRINT

Runxun Zhang, Jingwei Wei, Bo XU

Institute of Automation, Chinese Academy of Sciences
Beijing China

Yizhou Liu

Fudan University
Shanghai China

Li Dongrui

The second Hospital of Hebei Medical University
Hebei China

November 24, 2025

ABSTRACT

Deformable image registration (DIR) remains a fundamental yet challenging problem in medical image analysis, largely due to the prohibitively high-dimensional deformation space of dense displacement fields and the scarcity of voxel-level supervision. Existing reinforcement learning frameworks often project this space into coarse, low-dimensional representations, limiting their ability to capture spatially variant deformations. We propose MorphSeek, a fine-grained representation-level policy optimization paradigm that reformulates DIR as a spatially continuous optimization process in the latent feature space. MorphSeek introduces a stochastic Gaussian policy head atop the encoder to model a distribution over latent features, facilitating efficient exploration and coarse-to-fine refinement. The framework integrates unsupervised warm-up with weakly supervised fine-tuning through Group Relative Policy Optimization, where multi-trajectory sampling stabilizes training and improves label efficiency. Across three 3D registration benchmarks (OASIS brain MRI, LiTS liver CT, and Abdomen MRCT), MorphSeek achieves consistent Dice improvements over competitive baselines while maintaining high label efficiency with minimal parameter cost and low step-level latency overhead. Beyond optimizer specifics, MorphSeek advances a representation-level policy learning paradigm that achieves spatially coherent and data-efficient deformation optimization, offering a principled, backbone-agnostic, and optimizer-agnostic solution for scalable visual alignment in high-dimensional settings.

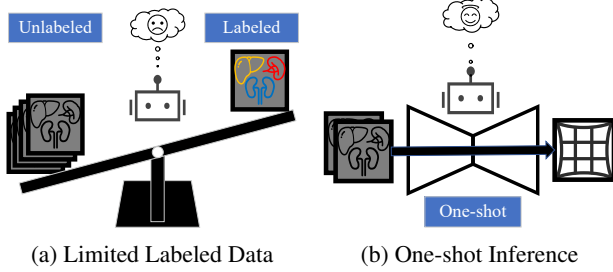


Figure 1: Two Major Challenges Faced by DL-based DIR

1 Introduction

Deformable image registration (DIR) is a highly challenging core task in medical image analysis[34, 49, 43]. Its goal is to establish voxel-wise spatial correspondences between two three-dimensional medical images, thereby enabling precise anatomical alignment. Owing to the pronounced non-rigid, large-scale deformations and inter-subject variability of anatomical structures, DIR is substantially more difficult than generic visual recognition tasks: it must achieve global structural alignment while preserving local geometric consistency[14]. Classical registration methods formulate DIR as a continuous optimization problem and solve for the deformation field via iterative procedures[1, 2, 45, 51], but their computational cost is extremely high[41, 35].

Driven by the rapid progress of deep learning[26, 52], recent approaches adopt end-to-end encoderdecoder architectures to directly map image pairs to deformation fields, achieving significant gains in both efficiency and accuracy[3, 6, 63, 38, 37, 33, 8].

Nevertheless, deep learningbased DIR still faces two obstacles: **(i)** it relies heavily on supervision signals despite extremely limited annotations in most medical scenarios, and **(ii)** the difficulty of mainstream single-shot inference schemes in handling complex large-deformation cases, which ultimately limits registration accuracy (Figure 1).

The first challenge is to reliably solve high-difficulty, large-deformation registration problems given only a very small number of labeled examples. Complex anatomical structures and large-scale non-rigid deformations often require fine-grained voxel-level supervision to be stably aligned. However, segmentation annotations are exceedingly scarce in most medical settings. As a result, most registration models are forced to rely on unsupervised losses based on image similarity[20, 21, 13, 61], whose ability to constrain local boundaries and subtle structures is limited. Existing works mainly strengthen unsupervised registration via pseudo-label generation[30, 54, 18], architectural refinements[58, 59, 24, 10], or new similarity metrics[16, 15], but comparatively little attention has been paid to maximizing supervision efficiency from a fixed yet very limited set of labels, especially for complex large-deformation cases.

The second challenge stems from the fact that most deep learningbased DIR models perform inference via a single forward pass, i.e., they predict the deformation field in one shot[3, 6, 10]. In scenarios involving large-scale non-rigid deformations, such as thoracic or abdominal registration, such models often fit only the global structural differences while struggling to reliably recover local boundaries and fine geometric details. To improve alignment under complex deformations, several methods introduce step-wise registration[22, 60, 62, 57, 42], decomposing a large deformation into a sequence of incremental updates to realize coarse-to-fine optimization. However, existing step-wise frameworks typically rely on manually designed, fixed cascaded structures and lack a learnable multi-step decision policy. Reinforcement learning (RL) has been explored for image registration because its stochastic, Markov decision process is naturally compatible with step-wise optimization. However, most existing RL-based registration methods are confined to low-dimensional rigid transformations[29, 31, 32, 40, 19, 50]. Directly treating a full 3D deformable field as the action space would make memory consumption and sampling cost prohibitive, severely limiting the applicability of RL to real-world deformable registration.

To address these issues, we propose MorphSeek, which reformulates deformable registration as latent-space policy optimization by introducing a sampleable high-resolution latent representation at the top encoder layer and treating it as the policy action, thereby avoiding RL reasoning directly in the million-dimensional deformation field while preserving fine spatial granularity. The framework first performs unsupervised warm-up to shape a stable latent space and then applies Group Relative Policy Optimization (GRPO) with multiple trajectories and multiple steps under weak supervision, repeatedly reusing scarce labels for coarse-to-fine refinement. To make such high-dimensional policies trainable, we further propose Latent-Dimension Variance Normalization (LDVN), which statistically controls the variance of log-likelihoods and yields stable, unbiased gradients for scalable 3D dense prediction.

Our main contributions are as follows:

- We introduce a new latent-space policy optimization paradigm for deformable image registration. By defining the policy distribution in the encoder latent feature space instead of operating directly on the dense deformation field, we realize a fine-grained, scalable, and backbone-agnostic step-wise optimization mechanism.
- We propose LDVN, the first general statistical normalization scheme that stabilizes GRPO in high-dimensional dense prediction settings. We show that LDVN controls the variance of the log-likelihood without altering the gradient direction or introducing bias, allowing GRPO to operate stably in high-dimensional 3D feature spaces and providing both

theoretical and practical support for applying RL to dense prediction tasks.

- We construct a highly label-efficient multi-trajectory, multi-step weakly supervised framework. Through warm-up pre-training and GRPO-guided coarse-to-fine refinement, our framework repeatedly reuses supervision signals under very limited annotations, markedly improving large-deformation registration quality while maintaining a comparable parameter count and acceptable inference latency.

2 Related Work

2.1 DL-Based Deformable Medical Image Registration

Early DL-based DIR methods were fully supervised using deformation vector fields (DVF)[48, 56, 53, 25, 47, 5]. After Hu et al. proposed using anatomical segmentations instead of DVF for supervision[20], such fully supervised strategies became less common. Since VoxelMorph[3], a U-Net-style CNN trainable in an unsupervised manner, subsequent studies have largely evolved within this unsupervised U-Net-style paradigm[38, 10, 37, 8, 6, 63].

Meanwhile, leveraging segmentation labels to further improve registration has become an active research direction. Hu et al. extended the label-driven idea and systematically discussed the advantages of segmentation-supervised training over purely unsupervised objectives[21]. Ferrante et al. used segmentation labels to guide the weighting of different similarity terms during registration[13]. Zhou et al. proposed macJNet[61], which jointly learns two segmentation networks and one registration network.

There have also been attempts to combine unsupervised and weakly-supervised learning. Li et al. combined segmentation-labeled and unlabeled image pairs for registration using consistency regularization in a student-teacher framework[28]. Unsupervised models such as VoxelMorph[3] often include hybrid objectives that combine image-similarity and label-based losses. Chen et al. proposed a training strategy that first performs unsupervised pretraining with randomly generated images and then fine-tunes on the target task, maintaining strong performance when domain-specific data are limited[7]. However, these approaches still do not simultaneously exploit both unlabeled and labeled data from the same domain to maximally optimize the registration model.

From another perspective, coarse-to-fine registration has been extensively explored. ULAE-Net[46] performs step-wise registration by repeatedly applying the network. LapIRN[42] cascades multiple Laplacian pyramid networks to implement coarse-to-fine alignment. However, these methods use fixed, deterministic schedules and lack adaptive exploration of optimal registration strategies.

2.2 Reinforcement Learning in DIR

In recent years, reinforcement learning (RL) has advanced rapidly in decision-making, robotics, and large-model reasoning[44, 11]. However, when applied to dense prediction tasks, the continuous and high-dimensional state and action spaces particularly in 3D lead to unstable training, high exploration cost, and substantial memory overhead; this bottleneck is especially pronounced in deformable image registration (DIR).

Krebs et al. proposed an agent-based non-rigid registration framework that reduces the DIR action space from dense DVFs to a statistical deformation model (PCA over B-spline parameterized deformations), significantly lowering the action dimensionality[25]. However, their method requires dense DVFs as supervision, which is impractical in contemporary settings. Luo et al. introduced SPAC[30], which compresses a pair into a 64-D plan and relies on an extra critic for stability (SAC-based), which complicates deployment. Moreover, the 64-D bottleneck discards spatial detail, limiting performance.

In summary, the central challenge for applying RL to DIR is how to retain model generality while effectively shifting exploration and optimization from the dense field to a low-dimensional, training-friendly space.

3 Method

MorphSeek is a training paradigm that can be generalized to any encoder-decoder-based registration model and provides a unified formulation of deformable registration via latent-space policy optimization. The paradigm consists of three stages: **(i)** an RL-friendly refactoring step that constructs a sampleable latent space at the top of the encoder and decouples the encoder and decoder, **(ii)** an unsupervised warm-up phase that shapes a stable latent-space structure, and **(iii)** a GRPO-based weakly supervised fine-tuning phase that performs coarse-to-fine policy updates with multiple trajectories and multiple steps so that the scarce labels can be repeatedly reused (Figure 2). For clarity of exposition, we instantiate MorphSeek with a U-Net backbone.

3.1 Refactoring Registration Networks for Latent Policy Learning

Deformable registration networks typically adopt a U-Net-style encoder-decoder architecture with skip connections. Given a moving image I_m and fixed image I_f both in $\mathbb{R}^{H \times W \times D}$, the network takes their concatenation $x = [I_m, I_f]$ as input. The encoder \mathcal{E} extracts multi-scale features:

$$\{\mathbf{f}_1, \mathbf{f}_2, \dots, \mathbf{f}_L\} = \mathcal{E}(x) \quad (1)$$

where $\mathbf{f}_l \in \mathbb{R}^{C_l \times H_l \times W_l \times D_l}$ denotes the feature at level l with progressively reduced spatial resolution. The de-

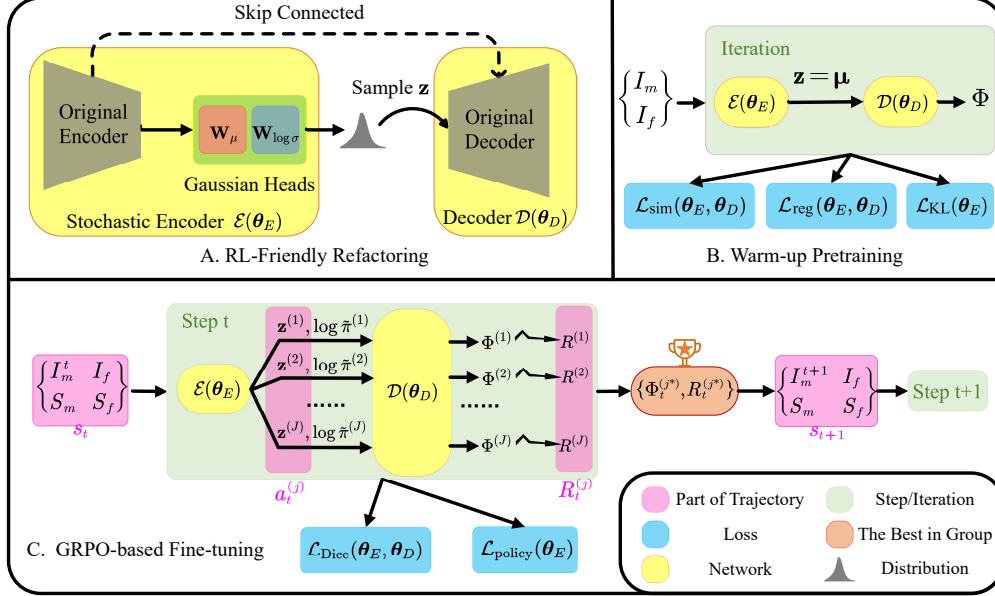


Figure 2: MorphSeek Registration Framework Process

coder \mathcal{D} then upsamples and fuses these features via skip connections to predict a dense deformation field:

$$\Phi = \mathcal{D}(\{\mathbf{f}_1, \mathbf{f}_2, \dots, \mathbf{f}_L\}) \in \mathbb{R}^{3 \times H \times W \times D} \quad (2)$$

where Φ represents per-voxel displacement vectors, yielding the warped image $I_m \circ \Phi$.

In a conventional deterministic encoder \mathcal{E} , the top-level feature \mathbf{f}_L is directly fed into the decoder \mathcal{D} . To enable RL-based fine-tuning, we decouple the encoder and decoder in the U-Net-style architecture (while preserving skip connections) and introduce stochasticity at the encoder output via Gaussian parameterization. This allows the encoder to model a probability distribution over latent vectors and supports policy optimization with Group Relative Policy Optimization (GRPO).

Specifically, we append two convolutional heads to the top-level feature $\mathbf{f}_L \in \mathbb{R}^{C_L \times H_L \times W_L \times D_L}$: a mean head \mathbf{W}_μ and a log-standard-deviation head $\mathbf{W}_{\log \sigma}$, both with kernel size 1, i.e., $\mathbf{W}_\mu, \mathbf{W}_{\log \sigma} \in \mathbb{R}^{C_L \times C_L \times 1 \times 1 \times 1}$.

These two heads take the tensor \mathbf{f}_L and parameterize a multivariate Gaussian $\mathcal{N}(\mu, \sigma^2)$. To stabilize training, we impose constraints and clipping on the outputs:

$$\mu = \tanh(\mathbf{W}_\mu(\mathbf{f}_L)) \cdot \lambda_{\text{scale}} \in \mathbb{R}^{C_L \times H_L \times W_L \times D_L} \quad (3)$$

$$\log \sigma = \text{clip}(\mathbf{W}_{\log \sigma}(\mathbf{f}_L), \sigma_{\min}, \sigma_{\max}) \in \mathbb{R}^{C_L \times H_L \times W_L \times D_L} \quad (4)$$

We further introduce a temperature parameter $\tau > 0$ to modulate exploration. During training, the latent vector is sampled using the reparameterization trick:

$$\mathbf{z} = \mu + \tau \cdot \boldsymbol{\sigma} \odot \boldsymbol{\epsilon}, \quad \boldsymbol{\epsilon} \sim \mathcal{N}(\mathbf{0}, \mathbf{I}) \quad (5)$$

Compared to Eq. 2, the inputoutput of the decoder is modified as:

$$\Phi = \mathcal{D}(\{\mathbf{f}_1, \mathbf{f}_2, \dots, \mathbf{f}_{L-1}, \mathbf{z}\}) \quad (6)$$

3.2 Warm-up Priors for Stable Policy Optimization

To ensure that the subsequent GRPO fine-tuning operates in a stable and well-conditioned latent space, we first pretrain the encoder and decoder on unlabeled data. Comparative analyses with and without warm-up are reported in Section 5.

During warm-up, to obtain stable warping estimates, we adopt a deterministic latent variable by setting $\tau = 0$, i.e.,

$$\mathbf{z} = \mu. \quad (7)$$

Let θ_E and θ_D denote the trainable parameters of the encoder and decoder, respectively, and let $\theta = \{\theta_E, \theta_D\}$. The overall warm-up objective minimizes an unsupervised loss composed of an image-similarity term, a deformation regularizer, and a KL penalty on the Gaussian heads:

$$\begin{aligned} \mathcal{L}_{\text{warm}}(\theta) = & \mathcal{L}_{\text{sim}}(I_f, I_{m \circ \Phi}) + \lambda_{\text{reg}} \mathcal{L}_{\text{reg}}(\Phi) \\ & + \beta_{\text{KL}} \mathcal{L}_{\text{KL}}(q_{\theta_E}(\mathbf{z} | \mathbf{f}_L) \| \mathcal{N}(\mathbf{0}, \mathbf{I})), \end{aligned} \quad (8)$$

where λ_{reg} and β_{KL} are weighting coefficients, and q_{θ_E} denotes the factorized Gaussian parameterized by the encoder. Each loss component can be instantiated in multiple ways; for this work, we use mean squared error (MSE), diffusion regularization, and standard KL divergence, with exact formulations detailed in the supplement.

3.3 Multi-Trajectory GRPO for Step-Wise Registration

After warm-up pretraining, we fine-tune the encoder-decoder with segmentation labels under the GRPO framework to further improve registration accuracy. In this stage, the encoders stochastic output distribution is treated as a policy, denoted by $\pi(\mathbf{z} \mid \mathbf{f}_L)$, where the state s_t is the current registration pair $\{I_m^{t-1}, I_f\}$ and the action a_t is the sampled latent \mathbf{z} . At each fine-tuning step t , we generate a group of trajectories per sample to enable exploration through encoder stochasticity.

For each trajectory $j = 1, \dots, J$, the decoder produces a single-step deformation field $\phi_t^{(j)}$ from the sampled latent $\mathbf{z}^{(j)}$, and we compute a scalar reward:

$$\begin{aligned} R^{(j)} &= w_{\text{Dice}} \cdot [\text{Dice}(S_f, S_{m \circ \Phi_t^{(j)}}) - \text{Dice}(S_f, S_{m \circ \Phi_{t-1}})] \\ &\quad + w_{\text{NJD}} \cdot \text{NJD}(\Phi_t^{(j)}), \end{aligned} \quad (9)$$

where $S_f, S_m \in \mathbb{R}^{K \times H \times W \times D}$ are the fixed and moving segmentation labels, and $\Phi_t^{(j)} = \Phi_{t-1} \circ \phi_t^{(j)}$. Here, NJD penalizes voxels with negative Jacobian determinants $|J_{\Phi_t^{(j)}}| < 0$, and $w_{\text{Dice}} > 0$, $w_{\text{NJD}} < 0$ are scalar weights.

To compute policy gradients, we perform group-wise normalization of the trajectory rewards for each sample, yielding the advantage

$$A^{(j)} = \frac{R^{(j)} - \bar{R}}{\sigma_R + \epsilon}, \quad (10)$$

where \bar{R} and σ_R are the mean and standard deviation of $\{R^{(j)}\}_{j=1}^J$ for the current sample, and $\epsilon = 10^{-8}$ prevents division by zero. We also compute the relative log-likelihood within the group:

$$\log \tilde{\pi}^{(j)} = \log \pi(\mathbf{z}^{(j)} \mid \boldsymbol{\mu}, \boldsymbol{\sigma}) - \overline{\log \pi}, \quad (11)$$

where $\boldsymbol{\mu}, \boldsymbol{\sigma}$ are the encoder outputs for the current state (shared across the J samples), and $\overline{\log \pi}$ is the group mean of $\log \pi(\mathbf{z}^{(j)} \mid \boldsymbol{\mu}, \boldsymbol{\sigma})$.

However, for conventional backbones[6, 38], we observe that the latent dimensionality \mathbf{z} (denoted as $N = C_L \times H_L \times W_L \times D_L$) often reaches tens of thousands, which is far larger than in typical GRPO applications. If we directly sum over all N positions when computing $\log \pi$, the variance of $\log \pi$ within each group will escalate rapidly with N . This leads to impaired exploration discriminability and unstable training.

To address this issue, we propose Latent-Dimension Variance Normalization (LDVN), which introduces a scaling factor s in the computation of $\log \pi$:

$$\begin{aligned} \log \pi(\mathbf{z} \mid \boldsymbol{\mu}, \boldsymbol{\sigma}) \\ = -\frac{1}{2s} \sum_{i=1}^N \left[\left(\frac{z_i - \mu_i}{\tau \sigma_i} \right)^2 + \log(2\pi\tau^2\sigma_i^2) \right]. \end{aligned} \quad (12)$$

Algorithm 1 GRPO-based Fine-tuning

```

Initialize: Load pretrained  $\theta = (\theta_E, \theta_D)$ , set  $\tau > 0$ 
for each pair  $\{I_m, I_f, S_m, S_f\}$  do
    Initialize:  $I_m^0 \leftarrow I_m$ 
    for each step  $t = 1, \dots, T$  do
        Sample  $\phi_t^{(1)}, \phi_t^{(2)}, \dots, \phi_t^{(J)}$ 
        Compute  $\Phi_t^{(j)} = \Phi_{t-1} \circ \phi_t^{(j)}$ 
        Compute  $R^{(j)}, A^{(j)}, \log \tilde{\pi}^{(j)}$ , and  $\mathcal{L}_{\text{grpo}}$ 
        Update  $\theta \leftarrow \theta - \eta \nabla_{\theta} \mathcal{L}_{\text{grpo}}$ 
        Update  $\Phi_t, I_m^t$  via Eqs. 17 and 18
    end for
end for

```

For different image resolutions and backbone architectures, we dynamically adjust s to constrain $\text{std}(\log \tilde{\pi}^{(j)})$ to a constant value. In doing so, we ensure statistical consistency with Eq. 10 and 11, thereby achieving stable policy updates while preserving fine-grained stochasticity.

We can prove the unbiasedness of L DVN through a simple derivation. For any $s > 0, b \in \mathbb{R}$,

$$\left(\frac{1}{s} \log \pi^{(j)} + b \right) - \left(\frac{1}{s} \log \pi + b \right) = \frac{1}{s} (\log \pi^{(j)} - \overline{\log \pi}). \quad (13)$$

Hence L DVN only rescales within-group relative log-likelihoods without changing their ordering or the gradient direction; when multiplied by the zero-mean advantage in Eq. 10, it is equivalent to a step-size rescaling, leaving the estimator unbiased. Note that L DVN is only applied to the statistics of $\log \pi$ in the policy loss, and does not participate in the reparameterization sampling of Eq. 5, thus it does not alter the sampling distribution of $\pi(\mathbf{z} \mid \boldsymbol{\mu}, \boldsymbol{\sigma})$ or the exploration temperature τ .

Regarding the specific value of s , we denote the summation terms in Eq. 12 as X_i . It can be proved that **a.** with bounded second moments and weak dependence, $\text{Var}(\sum_{i=1}^N X_i) = O(N)$, and **b.** choosing $s \propto \sqrt{N}$ keeps $\text{Var}(\frac{1}{s} \sum_{i=1}^N X_i) = O(1)$ and $\text{std}(\log \tilde{\pi}^{(j)}) = O(1)$. Therefore, the value of s is typically set to \sqrt{N} . (Detailed derivation is provided in the Appendix.)

In all, the policy loss is defined as

$$\mathcal{L}_{\text{policy}}(\theta_E) = -\frac{1}{J} \sum_{j=1}^J A^{(j)} \cdot \log \tilde{\pi}^{(j)}, \quad (14)$$

which updates the encoder parameters θ_E through the gradient of $\log \pi$, increasing the sampling probability of high-reward trajectories.

In parallel, we compute a supervised soft-Dice loss using differentiable warping:

$$\mathcal{L}_{\text{Dice}}(\theta) = \frac{1}{J} \sum_{j=1}^J \left[1 - \text{Dice}(S_f, S_{m \circ \Phi_t^{(j)}}) \right]. \quad (15)$$

Note that $\mathcal{L}_{\text{Dice}}$ is computed with soft labels via trilinear interpolation to ensure differentiability, whereas the reward in $\mathcal{L}_{\text{policy}}$ does not backpropagate gradients and is computed with hard labels to more faithfully reflect the task metric.

To prevent catastrophic forgetting of the representations learned during warm-up and to maintain smooth and physically plausible deformations, we retain the warm-up objective as a regularizer. It is computed through Eqs. 7 and 8 rather than sample averaging. The overall loss for GRPO fine-tuning is¹

$$\mathcal{L}_{\text{grpo}}(\theta) = \mathcal{L}_{\text{policy}}(\theta_E) + \lambda_{\text{warm}} \mathcal{L}_{\text{warm}}(\theta) + \lambda_{\text{Dice}} \mathcal{L}_{\text{Dice}}(\theta). \quad (16)$$

Unlike PPO/TRPO which bound consecutive policy ratios, we adopt a fixed-prior trust region by penalizing $\text{KL}(\pi_{\theta_E} \| \mathcal{N}(0, I))$ with a target-KL schedule. Warm-up already puts $\pi_{\theta_{E_0}}$ near $\mathcal{N}(0, I)$, so keeping this KL small bounds the drift to the warm-up policy while remaining critic-free and ratio-free in high-dimensional latents.

At the end of each step, we greedily select the trajectory with the highest reward to update the current state. Specifically, letting $j^* = \arg \max_j R^{(j)}$, we update the deformation field and moving image via

$$\Phi_t \leftarrow \Phi_{t-1} \circ \phi^{(j^*)}, \quad (17)$$

$$I_m^t \leftarrow I_{m \circ \Phi_t}. \quad (18)$$

The process is repeated for T steps or until convergence. The overall procedure is summarized in Algorithm 1.

4 Experiments

4.1 Datasets

We evaluate MorphSeek on three registration tasks spanning five 3D medical imaging datasets.

OASIS. A Learn2Reg[17] task for inter-patient brain MRI registration[36]. Volumes are preprocessed and resampled to $160 \times 192 \times 224$. From 414 training volumes, we form 400/100/20 pairs for pretraining/GRPO/validation. Test set: 19 official challenge validation pairs.

LiTS. Contains 131 contrast-enhanced abdominal CT scans[4]. We use whole-liver labels only. Volumes are resampled to $160 \times 192 \times 224$. Data split: 400/100/20/40 pairs for pretraining/GRPO/validation/test, with no test volume overlap in training.

¹The encoder parameterizes a Gaussian distribution $\mathcal{N}(\mu, \sigma^2)$ in both stages. During warm-up, we regularize it toward $\mathcal{N}(0, I)$ via the KL term in Eq. 8. In GRPO fine-tuning, this same KL divergence (evaluated with $\tau = 0$ as in warm-up) is retained to maintain a fixed-prior trust region.

Abdomen MR-CT. A Learn2Reg[17] task for intra-patient abdominal MR-CT registration using 8 paired scans from TCIA[9] and 90 unpaired scans from BCV[55] and CHAOS[23]. Volumes are resampled to $160 \times 192 \times 192$. From unpaired data, we construct 400/100/20 MR-CT pairs for pretraining/GRPO/validation. Test set: 8 official paired scans. For this cross-modality task we use the MIND descriptor[16] instead of MSE as the image similarity term.

4.2 Baselines and Implementations

We select three baseline algorithms for refactoring, namely VoxelMorph[3], TransMorph[6], and NICE-Trans[38], and we include two state-of-the-art frameworks CorrMLP[39], RIIR[57] and an RL-based framework SPAC[30], for comparison. To ensure fairness, each baseline is trained with the same weakly supervised setting and a Dice loss on segmentation labels. We also include WarpDDF+RegCut[28] which can combine segmentation labeled data and unlabeled data, as a comparison. Because most traditional optimization-based methods cannot effectively leverage label supervision under the same setting, we place their unsupervised training results in the supplementary materials.

We additionally adopt a widened VoxelMorph variant (VoxelMorph-L) with channels [32, 64, 128, 256, 256] (approximately 27M parameters) to provide a sufficiently expressive latent space for GRPO. We also use VoxelMorph-L as the baseline.

Training uses Adam (1e-4) and batch size 1; other hyper-parameters and hardware details are in the supplement.

We report Dice[12] (%) for segmentation overlap and the percentage of voxels with negative Jacobian determinant (NJD[27], %) for deformation regularity.

5 Results and Analysis

5.1 Overall Performance Across Tasks and Backbones

As summarized in Fig. 3 and Table 1, MorphSeek consistently improves Dice and reduces NJD across three 3D benchmarks and three backbones (VoxelMorph-L, TransMorph, and NICE-Trans). On OASIS, Dice increases by 23% while NJD decreases by roughly one-third relative to the corresponding baselines; on the more challenging cross-modality Abdomen MR- \leftarrow CT task, MorphSeek yields more than a 4% Dice gain and nearly halves NJD for TransMorph. Most gains are statistically significant under the Wilcoxon signed-rank test ($p < 0.05$), indicating that latent-space policy optimization benefits both small-deformation brain MRI registration and large-deformation cross-modality scenarios in terms of global alignment and local regularity.

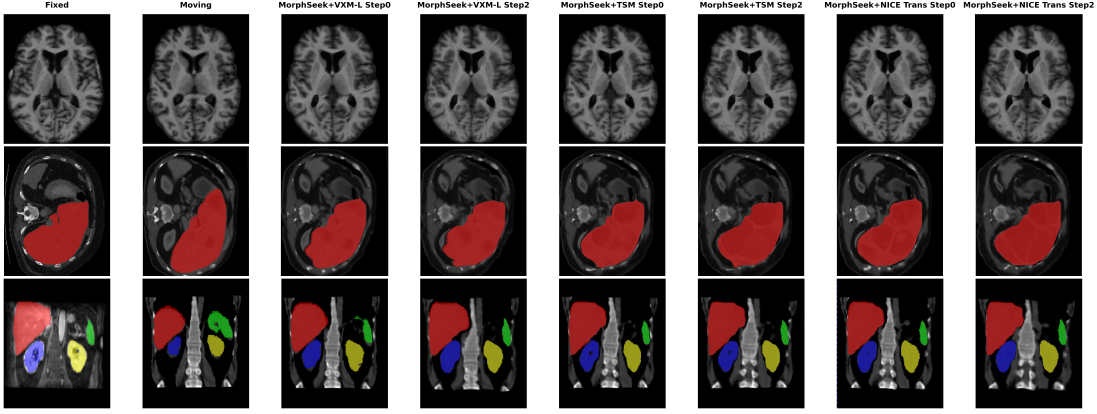


Figure 3: The Performance of MorphSeek Across Three Different Tasks. Labels are overlaid only for the two abdominal datasets; OASIS is left unlabeled to avoid clutter from its 35 foreground classes.

Table 1: Quantitative comparison on three registration tasks. All methods except affine **use weakly supervised training**. \uparrow : higher is better; \downarrow : lower is better. Our results are shown in bold and marked with * if there is a statistically significant difference ($p < 0.05$) from their baselines by a Wilcoxon signed-rank test. In MorphSeek, both Trajs/Steps are set to 6/3. NJDs in SPAC cannot be calculated due to coupling in the deformation field; see appendix.

Method	OASIS (Brain MRI)		LiTS (Liver CT)		Abdomen MR \leftarrow CT	
	Mean Dice (%) \uparrow	NJD (%) \downarrow	Dice (%) \uparrow	NJD (%) \downarrow	Mean Dice (%) \uparrow	NJD (%) \downarrow
Only Affine	58.52 \pm 4.08	–	60.21 \pm 10.04	–	37.82 \pm 18.11	–
CorrMLP [39]	88.35 \pm 1.33	0.08 \pm 0.03	89.22 \pm 3.08	0.25 \pm 0.11	86.82 \pm 5.05	0.49 \pm 0.41
RIIR [57] (Steps=12)	87.76 \pm 2.55	0.12 \pm 0.02	88.95 \pm 4.16	0.33 \pm 0.11	80.73 \pm 4.31	1.06 \pm 0.81
WarpDDF+RegCut [28]	86.64 \pm 3.83	0.26 \pm 0.06	85.57 \pm 3.99	0.61 \pm 0.18	85.49 \pm 8.21	1.11 \pm 0.57
SPAC [30] (Steps=20)	78.92 \pm 5.31	N/A	75.38 \pm 8.39	N/A	69.29 \pm 10.13	N/A
VoxelMorph-L [3] + MorphSeek (Ours)	84.77 \pm 2.49 87.16\pm1.97*	0.15 \pm 0.12 0.10\pm0.02*	84.97 \pm 6.37 88.99\pm3.11*	0.73 \pm 0.16 0.24\pm0.08*	77.96 \pm 9.15 82.44\pm6.37*	1.05 \pm 0.64 0.57\pm0.39*
TransMorph [6] + MorphSeek (Ours)	85.89 \pm 1.40 88.89\pm1.82*	0.16 \pm 0.09 0.06\pm0.02*	88.31 \pm 5.33 90.11\pm4.75*	0.46 \pm 0.15 0.16\pm0.09*	82.37 \pm 4.87 86.49\pm3.35*	0.84 \pm 0.47 0.35\pm0.22*
NICE-Trans [38] + MorphSeek (Ours)	86.79 \pm 2.39 89.02\pm1.45*	0.02 \pm 0.01 0.02\pm0.01	88.42 \pm 3.96 90.47\pm3.65*	0.17 \pm 0.08 0.16\pm0.09	83.19 \pm 3.85 86.51\pm2.97*	0.36 \pm 0.14 0.32\pm0.17*

Table 2: Ablation study on trajectory number and refinement steps on OASIS dataset. Using TransMorph + MorphSeek. Each cell shows Dice (%) ↑ / NJD (%) ↓.

Trajs \ Steps	1	2	3	4
2	86.71 / 0.08	87.13 / 0.08	87.78 / 0.08	87.94 / 0.08
4	86.89 / 0.07	87.96 / 0.06	88.26 / 0.06	88.14 / 0.08
6	87.67 / 0.06	88.72 / 0.05	88.89 / 0.06	88.51 / 0.07
8	OOM Error	N/A	N/A	N/A

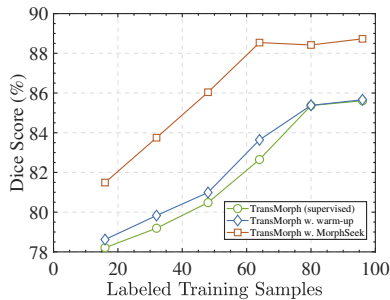


Figure 4: Impact of Warm-up and MorphSeek on GRPO Fine-tuning Performance with Limited Labeled Data (OASIS dataset)

5.2 Policy & Label Efficiency Ablation

The ablation on trajectory number and refinement steps on OASIS (Table 2) reveals a clear pattern. Increasing the number of trajectories up to six yields a steady improvement in Dice and a decrease in NJD, while adding refinement steps from one to three also brings consistent gains. Beyond three steps, however, the benefits saturate and the deformation field starts to show artifacts, reflected by degraded NJD and local distortions.

This behavior is consistent with the intended coarse-to-fine design: the first step focuses on establishing coarse alignment, whereas subsequent steps repeatedly enforce local constraints under the same labels, effectively reusing weak supervision. When the data have already been fully exploited, additional steps no longer help and instead tend to compromise the physical plausibility of the deformation. Moreover, attempting more than 8 trajectories leads to out-of-memory errors, which matches the increased sampling cost in a high-dimensional policy space.

MorphSeek is particularly advantageous in weakly supervised settings with very limited labels (Fig. 4). Using TransMorph as the backbone, MorphSeek already achieves strong gains with only about 16 labeled pairs and approaches its full-label performance with roughly 60 pairs. Notably, MorphSeek achieves 98.5% of its full-label performance using only 60% of the training data, while the baseline TransMorph requires 80% of labels to reach a comparable level.

These observations support our interpretation that the multi-trajectory, multi-step GRPO scheme effectively reuses each labeled pair multiple times along the refine-

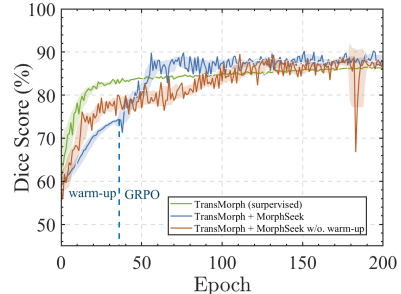


Figure 5: Validation Dice on OASIS: Effect of Warm-up Before GRPO (TransMorph Backbone), where the dotted line marks the switch from warm-up to GRPO

ment steps, substantially improving the label efficiency of weak supervision and raising the performance ceiling in complex registration tasks.

5.3 Computational Overhead and the Role of Warm-up

Table 4 analyzes the structural and runtime overhead introduced by the RL-friendly refactoring. For all three backbones, the additional parameters are below 3% and single-step inference latency remains almost unchanged. Multi-step inference exhibits roughly linear growth in runtime (about threefold latency for three refinement steps), which is expected for a cascaded scheme and enables a simple trade-off between accuracy and computational budget at deployment time.

The training curves on OASIS (Figure 5) highlight the critical role of unsupervised warm-up. Without warm-up, GRPO training is prone to oscillating policy gradients, higher sensitivity to hyperparameters, and a greater risk of non-physical deformations. With warm-up, the model typically reaches the same target Dice in roughly half the fine-tuning epochs and exhibits much smoother validation curves.

We therefore position warm-up as a prior-shaping and cost-reduction stage: it does not necessarily raise the ultimate performance ceiling, but substantially reduces the time, computational resources, and instability risks required to reach a given accuracy level, by pre-aligning the latent space before policy optimization.

5.4 Independent and Synergistic Contributions of MorphSeek Components

The component-wise ablation on OASIS (Table 3) clarifies the contribution of each part of MorphSeek. Adding only the Gaussian head barely changes performance, validating the lightweight nature of the RL-friendly refactoring. Introducing weakly supervised Dice loss significantly boosts Dice but has limited impact on NJD, indicating that, without high-dimensional policy optimization, the available supervision signal is not fully exploited.

Table 3: Ablation analysis of MorphSeek components on OASIS dataset.

#	Configuration	Sample encoder f_L ?	Weak Supervision?	Step/Traj	VoxelMorph-L		TransMorph		NICE-Trans	
					Mean Dice (%) ↑	NJD (%) ↓	Mean Dice (%) ↑	NJD (%) ↓	Mean Dice (%) ↑	NJD (%) ↓
1	Baseline	✗	✗	1/-	75.31±3.76	0.09±0.03	76.84±3.58	0.12±0.04	80.03±2.19	0.04±0.01
2	+ Gaussian head	✓	✗	1/-	75.64±3.69	0.09±0.02	76.79±3.69	0.12±0.04	80.20±2.37	0.04±0.01
3	+ Dice loss	✓	✓	1/-	84.87±2.01	0.32±0.10	86.08±1.67	0.29±0.14	86.81±1.99	0.21±0.08
4	+ Multi-step	✓	✓	3/-	85.50±2.33	0.37±0.13	86.37±1.39	0.35±0.15	87.06±1.82	0.23±0.09
5	+ GRPO (full)	✓	✓	3/6	87.16±1.97	0.10±0.02	88.89±1.82	0.06±0.02	89.02±1.45	0.02±0.01

Table 4: Efficiency analysis of RL-friendly refactoring on OASIS task. Inference time: averaged over five runs on the test set.

Baseline	Model Parameters			GPU Inference Time (ms)	
	Original	+Δ Abs	+Δ Rel	Original	+MorphSeek 1/2/3 step(s)
VoxelMorph-L	27.05M	+0.13M	+0.48%	625	685 / 1387 / 2022
TransMorph	46.77M	+1.18M	+2.53%	401	444 / 900 / 1376
NICE-Trans	5.71M	+0.13M	+2.27%	406	431 / 864 / 1295

The full MorphSeek configuration Gaussian head, multi-trajectory multi-step GRPO, and LDVN achieves simultaneous improvements in both Dice and NJD across all three backbones. This demonstrates that GRPO is the key mechanism that tightly couples weak supervision with multi-step registration. In particular, the combination of latent-space policy modeling, LDVN, and multi-step GRPO yields a stable and efficient optimization scheme that lifts the performance ceiling of deformable registration.

Across tasks, modalities, and architectures, MorphSeek delivers systematic quantitative gains, with Dice improvements on the order of 24% and NJD reductions of roughly 3060%, while also exhibiting clear advantages under low-label and resource-constrained settings. These results establish latent-space policy optimization as a practical and effective paradigm for 3D dense deformable registration.

6 Conclusion

We have presented MorphSeek, which reframes deformable image registration as latent-space policy optimization and stabilizes high-dimensional GRPO through Latent-Dimension Variance Normalization (LDVN). By shifting exploration from voxel-level deformation fields to a structured latent space, MorphSeek overcomes the dimensionality and computational bottlenecks that have limited RL-based registration to low-dimensional rigid transforms. Combined with unsupervised warm-up and multi-trajectory, multi-step GRPO refinement, it consistently improves Dice while reducing NJD across three 3D benchmarks and multiple backbones, with only marginal parameter and runtime overhead, making RL-based deformable registration practical under realistic memory and label budgets. Future work includes adaptive scheduling of refinement depth, incorporating stronger physical priors on deformations, and extending latent-space policy optimization to other dense correspondence problems.

References

- [1] B.B. Avants, C.L. Epstein, M. Grossman, and J.C. Gee. Symmetric diffeomorphic image registration with cross-correlation: Evaluating automated labeling of elderly and neurodegenerative brain. *Medical Image Analysis*, 12(1):26–41, 2008. Special Issue on The Third International Workshop on Biomedical Image Registration WBIR 2006.
- [2] Ruzena Bajcsy and Stane Kovai. Multiresolution elastic matching. *Computer Vision, Graphics, and Image Processing*, 46(1):1–21, 1989.
- [3] Guha Balakrishnan, Amy Zhao, Mert R. Sabuncu, John Guttag, and Adrian V. Dalca. Voxelmorph: A learning framework for deformable medical image registration. *IEEE Transactions on Medical Imaging*, 38(8):1788–1800, August 2019.
- [4] Patrick Bilic, Patrick Christ, Hongwei Bran Li, Eugene Vorontsov, Avi Ben-Cohen, Georgios Kaassis, Adi Szeskin, Colin Jacobs, Gabriel Efrain Humpire Mamani, Gabriel Chartrand, et al. The liver tumor segmentation benchmark (lits). *Medical Image Analysis*, 84:102680, 2023.
- [5] Xiaohuan Cao, Jianhua Yang, Li Wang, Zhong Xue, Qian Wang, and Dinggang Shen. Deep learning based inter-modality image registration supervised by intra-modality similarity, 2018.
- [6] Junyu Chen, Eric C. Frey, Yufan He, William P. Segars, Ye Li, and Yong Du. Transmorph: Transformer for unsupervised medical image registration. *Medical Image Analysis*, 82:102615, November 2022.
- [7] Junyu Chen, Shuwen Wei, Yihao Liu, Aaron Carass, and Yong Du. Pretraining deformable image registration networks with random images, 2025.
- [8] Zeyuan Chen, Yuanjie Zheng, and James C. Gee. Transmatch: A transformer-based multilevel dual-stream feature matching network for unsupervised deformable image registration. *IEEE Transactions on Medical Imaging*, 43(1):15–27, 2024.
- [9] K Clark, B Vendt, K Smith, J Freymann, J Kirby, P Koppel, S Moore, S Phillips, D Maffitt, M Pringle, L Tarbox, and F Prior. The cancer imaging archive (tcia): maintaining and operating a public information repository. *J Digit Imaging*, 26(6):1045–1057, Dec 2013.
- [10] Adrian V. Dalca, Guha Balakrishnan, John V. Guttag, and Mert R. Sabuncu. Unsupervised learning for

- fast probabilistic diffeomorphic registration. *CoRR*, abs/1805.04605, 2018.
- [11] DeepSeek-AI, Daya Guo, Dejian Yang, Haowei Zhang, Junxiao Song, Ruoyu Zhang, Runxin Xu, Qihao Zhu, Shirong Ma, Peiyi Wang, Xiao Bi, Xiaokang Zhang, Xingkai Yu, Yu Wu, Z. F. Wu, Zhibin Gou, Zhihong Shao, Zhuoshu Li, Ziyi Gao, Aixin Liu, Bing Xue, Bingxuan Wang, Bochao Wu, Bei Feng, Chengda Lu, Chenggang Zhao, Chengqi Deng, Chenyu Zhang, Chong Ruan, Damai Dai, Deli Chen, Dongjie Ji, Erhang Li, Fangyun Lin, Fucong Dai, Fuli Luo, Guangbo Hao, Guanting Chen, Guowei Li, H. Zhang, Han Bao, Hanwei Xu, Haocheng Wang, Honghui Ding, Huajian Xin, Huazuo Gao, Hui Qu, Hui Li, Jianzhong Guo, Jiashi Li, Jiawei Wang, Jingchang Chen, Jingyang Yuan, Junjie Qiu, Junlong Li, J. L. Cai, Jiaqi Ni, Jian Liang, Jin Chen, Kai Dong, Kai Hu, Kaige Gao, Kang Guan, Kexin Huang, Kuai Yu, Lean Wang, Lecong Zhang, Liang Zhao, Litong Wang, Liyue Zhang, Lei Xu, Leyi Xia, Mingchuan Zhang, Minghua Zhang, Minghui Tang, Meng Li, Miaojun Wang, Mingming Li, Ning Tian, Panpan Huang, Peng Zhang, Qiancheng Wang, Qinyu Chen, Qiushi Du, Ruiqi Ge, Ruisong Zhang, Ruizhe Pan, Runji Wang, R. J. Chen, R. L. Jin, Ruyi Chen, Shanghao Lu, Shangyan Zhou, Shanhua Chen, Shengfeng Ye, Shiyu Wang, Shuiping Yu, Shunfeng Zhou, Shuting Pan, S. S. Li, Shuang Zhou, Shaoqing Wu, Shengfeng Ye, Tao Yun, Tian Pei, Tianyu Sun, T. Wang, Wangding Zeng, Wanjia Zhao, Wen Liu, Wenfeng Liang, Wenzhong Gao, Wenqin Yu, Wentao Zhang, W. L. Xiao, Wei An, Xiaodong Liu, Xiaohan Wang, Xiaokang Chen, Xiaotao Nie, Xin Cheng, Xin Liu, Xin Xie, Xingchao Liu, Xinyu Yang, Xinyuan Li, Xuecheng Su, Xuheng Lin, X. Q. Li, Xiangyue Jin, Xiaojin Shen, Xiaosha Chen, Xiaowen Sun, Xiaoxiang Wang, Xinnan Song, Xinyi Zhou, Xianzu Wang, Xinxia Shan, Y. K. Li, Y. Q. Wang, Y. X. Wei, Yang Zhang, Yanhong Xu, Yao Li, Yao Zhao, Yaofeng Sun, Yaohui Wang, Yi Yu, Yichao Zhang, Yifan Shi, Yiliang Xiong, Ying He, Yishi Piao, Yisong Wang, Yixuan Tan, Yiyang Ma, Yiyuan Liu, Yongqiang Guo, Yuan Ou, Yuduan Wang, Yue Gong, Yuheng Zou, Yujia He, Yunfan Xiong, Yuxiang Luo, Yuxiang You, Yuxuan Liu, Yuyang Zhou, Y. X. Zhu, Yanhong Xu, Yanping Huang, Yaohui Li, Yi Zheng, Yuchen Zhu, Yunxian Ma, Ying Tang, Yukun Zha, Yuting Yan, Z. Z. Ren, Zehui Ren, Zhangli Sha, Zhe Fu, Zhean Xu, Zhenda Xie, Zhengyan Zhang, Zhewen Hao, Zhicheng Ma, Zhigang Yan, Zhiyu Wu, Zihui Gu, Zijia Zhu, Zijun Liu, Zilin Li, Ziwei Xie, Ziyang Song, Zizheng Pan, Zhen Huang, Zhipeng Xu, Zhongyu Zhang, and Zhen Zhang. Deepseek-r1: Incentivizing reasoning capability in llms via reinforcement learning, 2025.
- [12] Lee R. Dice. Measures of the amount of ecologic association between species. *Ecology*, 26(3):297–302, 1945.
- [13] Enzo Ferrante, Puneet Kumar Dokania, Rafael Marini Silva, and Nikos Paragios. Weakly supervised learning of metric aggregations for deformable image registration. *IEEE Journal of Biomedical and Health Informatics*, 23(4):1374–1384, 2019.
- [14] Yabo Fu, Yang Lei, Tonghe Wang, Walter J Curran, Tian Liu, and Xiaofeng Yang. Deep learning in medical image registration: a review. *Physics in Medicine & Biology*, 65(20):20TR01, October 2020.
- [15] G Haskins, J Kruecker, U Kruger, S Xu, PA Pinto, BJ Wood, and P Yan. Learning deep similarity metric for 3d mr-trus image registration. *Int J Comput Assist Radiol Surg*, 14(3):417–425, Mar 2019.
- [16] MP Heinrich, M Jenkinson, M Bhushan, T Matin, FV Gleeson, SM Brady, and JA Schnabel. Mind: modality independent neighbourhood descriptor for multi-modal deformable registration. *Med Image Anal*, 16(7):1423–1435, Oct 2012.
- [17] Alessa Hering, Lasse Hansen, Tony CW Mok, Albert CS Chung, et al. Learn2reg: comprehensive multi-task medical image registration challenge, dataset and evaluation in the era of deep learning. *IEEE Transactions on Medical Imaging*, 42(3):697–712, 2022.
- [18] M Hoffmann, B Billot, DN Greve, JE Iglesias, B Fischl, and AV Dalca. Synthmorph: Learning contrast-invariant registration without acquired images. *IEEE Trans Med Imaging*, 41(3):543–558, Mar 2022.
- [19] Jing Hu, Ziwei Luo, Xin Wang, Shanhui Sun, Youbing Yin, Kunlin Cao, Qi Song, Siwei Lyu, and Xi Wu. End-to-end multimodal image registration via reinforcement learning. *Medical Image Analysis*, 68:101878, 2021.
- [20] Yipeng Hu, Marc Modat, Eli Gibson, Nooshin Ghavami, Ester Bonmati, Caroline M. Moore, Mark Emberton, J. Alison Noble, Dean C. Barratt, and Tom Vercauteren. Label-driven weakly-supervised learning for multimodal deformable image registration. In *2018 IEEE 15th International Symposium on Biomedical Imaging (ISBI 2018)*. IEEE, April 2018.
- [21] Yipeng Hu, Marc Modat, Eli Gibson, Wenqi Li, Nooshin Ghavami, Ester Bonmati, Guotai Wang, Steven Bandula, Caroline M. Moore, Mark Emberton, Sébastien Ourselin, J. Alison Noble, Dean C. Barratt, and Tom Vercauteren. Weakly-supervised convolutional neural networks for multimodal image registration. *CoRR*, abs/1807.03361, 2018.
- [22] Xi Jia, Alexander Thorley, Wei Chen, Huaqi Qiu, Linlin Shen, Iain B. Styles, Hyung Jin Chang, Ales Leonardis, Antonio de Marvao, Declan P. O'Regan, Daniel Rueckert, and Jinming Duan. Learning a model-driven variational network for deformable image registration. *CoRR*, abs/2105.12227, 2021.

- [23] A. Emre Kavur, N. Sinem Gezer, Mustafa Bar, Sinem Aslan, Pierre-Henri Conze, Vladimir Groza, Duc Duy Pham, Soumick Chatterjee, Philipp Ernst, Sava Özkan, Bora Baydar, Dmitry Lachinov, Shuo Han, Josef Pauli, Fabian Isensee, Matthias Perkonigg, Rachana Sathish, Ronnie Rajan, Debdoott Sheet, Gurbandurdy Dovletov, Oliver Speck, Andreas Nürnberg, Klaus H. Maier-Hein, Gözde Bozda Akar, Gözde Ünal, Ouz Dicle, and M. Alper Selver. Chaos challenge - combined (ct-mr) healthy abdominal organ segmentation. *Medical Image Analysis*, 69:101950, April 2021.
- [24] Boah Kim, Jieun Kim, June-Goo Lee, Dong Hwan Kim, Seong Ho Park, and Jong Chul Ye. Unsupervised deformable image registration using cycle-consistent CNN. *CoRR*, abs/1907.01319, 2019.
- [25] Julian Krebs, Tommaso Mansi, Hervé Delingette, Li Zhang, Florin C. Ghesu, Shun Miao, Andreas K. Maier, Nicholas Ayache, Rui Liao, and Ali Kamen. Robust non-rigid registration through agent-based action learning. In Maxime Descoteaux, Lena Maier-Hein, Alfred M. Franz, Pierre Jannin, D. Louis Collins, and Simon Duchesne, editors, *Medical Image Computing and Computer Assisted Intervention - MICCAI 2017 - 20th International Conference, Quebec City, QC, Canada, September 11-13, 2017, Proceedings, Part I*, volume 10433 of *Lecture Notes in Computer Science*, pages 344–352. Springer, 2017.
- [26] Alex Krizhevsky, Ilya Sutskever, and Geoffrey E. Hinton. Imagenet classification with deep convolutional neural networks. *Commun. ACM*, 60(6):8490, May 2017.
- [27] Dongyang Kuang. On reducing negative jacobian determinant of the deformation predicted by deep registration networks. *CoRR*, abs/1907.00068, 2019.
- [28] Yiwen Li, Yunguan Fu, Iani J. M. B. Gayo, Qianye Yang, Zhe Min, Shaheer U. Saeed, Wen Yan, Yipei Wang, J. Alison Noble, Mark Emberton, Matthew J. Clarkson, Dean C. Barratt, Victor A. Prisacariu, and Yipeng Hu. Semi-weakly-supervised neural network training for medical image registration, 2024.
- [29] Rui Liao, Shun Miao, Pierre de Tournemire, Sasa Grbic, Ali Kamen, Tommaso Mansi, and Dorin Comaniciu. An artificial agent for robust image registration. *CoRR*, abs/1611.10336, 2016.
- [30] Ziwei Luo, Jing Hu, Xin Wang, Shu Hu, Bin Kong, Youbing Yin, Qi Song, Xi Wu, and Siwei Lyu. Stochastic planner-actor-critic for unsupervised deformable image registration. In *Proceedings of the AAAI Conference on Artificial Intelligence*, volume 36, pages 1917–1925, 2022.
- [31] Ziwei Luo, Xin Wang, Xi Wu, Youbing Yin, Kunlin Cao, Qi Song, and Jing Hu. A spatiotemporal agent for robust multimodal registration. *IEEE Access*, 8:75347–75358, 2020.
- [32] Kai Ma, Jiangping Wang, Vivek Singh, Birgi Tamersoy, Yao-Jen Chang, Andreas Wimmer, and Terrence Chen. Multimodal image registration with deep context reinforcement learning. In Maxime Descoteaux, Lena Maier-Hein, Alfred Franz, Pierre Jannin, D. Louis Collins, and Simon Duchesne, editors, *Medical Image Computing and Computer Assisted Intervention 2017*, pages 240–248, Cham, 2017. Springer International Publishing.
- [33] Tai Ma, Xinru Dai, Suwei Zhang, and Ying Wen. Pivit: Large deformation image registration with pyramid-iterative vision transformer. In Hayit Greenspan, Anant Madabhushi, Parvin Mousavi, Septimiu Salcudean, James Duncan, Tanveer Syeda-Mahmood, and Russell Taylor, editors, *Medical Image Computing and Computer Assisted Intervention – MICCAI 2023*, pages 602–612, Cham, 2023. Springer Nature Switzerland.
- [34] J.B. Antoine Maintz and Max A. Viergever. A survey of medical image registration. *Medical Image Analysis*, 2(1):1–36, 1998.
- [35] Lucas Mansilla, Diego H. Milone, and Enzo Ferante. Learning deformable registration of medical images with anatomical constraints. *Neural Networks*, 124:269–279, 2020.
- [36] DS Marcus, TH Wang, J Parker, JG Csernansky, JC Morris, and RL Buckner. Open access series of imaging studies (oasis): cross-sectional mri data in young, middle aged, nondemented, and demented older adults. *J Cogn Neurosci*, 19(9):1498–1507, Sep 2007.
- [37] Mingyuan Meng, Lei Bi, Dagan Feng, and Jinman Kim. *Non-iterative Coarse-to-Fine Registration Based on Single-Pass Deep Cumulative Learning*, page 8897. Springer Nature Switzerland, 2022.
- [38] Mingyuan Meng, Lei Bi, Michael Fulham, Dagan Feng, and Jinman Kim. *Non-iterative Coarse-to-Fine Transformer Networks for Joint Affine and Deformable Image Registration*, page 750760. Springer Nature Switzerland, 2023.
- [39] Mingyuan Meng, Dagan Feng, Lei Bi, and Jinman Kim. Correlation-aware coarse-to-fine mlps for deformable medical image registration. In *IEEE/CVF Conference on Computer Vision and Pattern Recognition (CVPR)*, pages 9645–9654, 2024.
- [40] Shun Miao and Rui Liao. *Agent-Based Methods for Medical Image Registration*, pages 323–345. Springer International Publishing, Cham, 2019.
- [41] Marc Modat, Gerard R. Ridgway, Zeike A. Taylor, Manja Lehmann, Josephine Barnes, David J. Hawkes, Nick C. Fox, and Sébastien Ourselin. Fast free-form deformation using graphics processing units. *Computer Methods and Programs in Biomedicine*, 98(3):278–284, 2010. HP-MICCAI 2008.

- [42] Tony C. W. Mok and Albert C. S. Chung. Large deformation diffeomorphic image registration with laplacian pyramid networks, 2020.
- [43] J.P.W. Pluim, J.B.A. Maintz, and M.A. Viergever. Mutual-information-based registration of medical images: a survey. *IEEE Transactions on Medical Imaging*, 22(8):986–1004, 2003.
- [44] Zhihong Shao, Peiyi Wang, Qihao Zhu, Runxin Xu, Junxiao Song, Xiao Bi, Haowei Zhang, Mingchuan Zhang, Y. K. Li, Y. Wu, and Daya Guo. Deepseekmath: Pushing the limits of mathematical reasoning in open language models, 2024.
- [45] Dinggang Shen and C. Davatzikos. Hammer: hierarchical attribute matching mechanism for elastic registration. *IEEE Transactions on Medical Imaging*, 21(11):1421–1439, 2002.
- [46] Yucheng Shu, Hao Wang, Bin Xiao, Xiuli Bi, and Weisheng Li. Medical image registration based on uncoupled learning and accumulative enhancement. In Marleen de Bruijne, Philippe C. Cattin, Stéphane Cotin, Nicolas Padov, Stefanie Speidel, Yefeng Zheng, and Caroline Essert, editors, *Medical Image Computing and Computer Assisted Intervention – MICCAI 2021*, pages 3–13, Cham, 2021. Springer International Publishing.
- [47] Hessam Sokooti, Bob de Vos, Floris Berendsen, Mohsen Ghafoorian, Sahar Yousefi, Boudewijn P. F. Lelieveldt, Ivana Isgum, and Marius Staring. 3d convolutional neural networks image registration based on efficient supervised learning from artificial deformations, 2019.
- [48] Hessam Sokooti, Bob de Vos, Floris Berendsen, Boudewijn P. F. Lelieveldt, Ivana Isgum, and Marius Staring. Nonrigid image registration using multi-scale 3d convolutional neural networks. In Maxime Descoteaux, Lena Maier-Hein, Alfred Franz, Pierre Jannin, D. Louis Collins, and Simon Duchesne, editors, *Medical Image Computing and Computer Assisted Intervention 2017*, pages 232–239, Cham, 2017. Springer International Publishing.
- [49] Aristeidis Sotiras, Christos Davatzikos, and Nikos Paragios. Deformable medical image registration: A survey. *IEEE Transactions on Medical Imaging*, 32(7):1153–1190, 2013.
- [50] Shanhai Sun, Jing Hu, Mingqing Yao, Jinrong Hu, Xiaodong Yang, Qi Song, and Xi Wu. Robust multimodal image registration using deep recurrent reinforcement learning. In C. V. Jawahar, Hongdong Li, Greg Mori, and Konrad Schindler, editors, *Computer Vision – ACCV 2018*, pages 511–526, Cham, 2019. Springer International Publishing.
- [51] Raj Varadhan, Grigorios Karangelis, Karthik Krishnan, and Susanta Hui. A framework for deformable image registration validation in radiotherapy clinical applications. *Journal of Applied Clinical Medical Physics*, 14(1):192–213, 01 2013.
- [52] Ashish Vaswani, Noam Shazeer, Niki Parmar, Jakob Uszkoreit, Llion Jones, Aidan N. Gomez, Łukasz Kaiser, and Illia Polosukhin. Attention is all you need. *CoRR*, abs/1706.03762, 2017.
- [53] Jian Wang and Miaomiao Zhang. Deepflash: An efficient network for learning-based medical image registration, 2020.
- [54] Yuelin Xin, Yicheng Chen, Shengxiang Ji, Kun Han, and Xiaohui Xie. On-the-Fly Guidance Training for Medical Image Registration. *arXiv e-prints*, page arXiv:2308.15216, August 2023.
- [55] Z Xu, CP Lee, MP Heinrich, M Modat, D Rueckert, S Ourselin, RG Abramson, and BA Landman. Evaluation of six registration methods for the human abdomen on clinically acquired ct. *IEEE Trans Biomed Eng*, 63(8):1563–1572, Aug 2016.
- [56] Xiao Yang, Roland Kwitt, and Marc Niethammer. Fast predictive image registration. In Gustavo Carneiro, Diana Mateus, Loïc Peter, Andrew Bradley, João Manuel R. S. Tavares, Vasileios Bellagiannis, João Paulo Papa, Jacinto C. Nascimento, Marco Loog, Zhi Lu, Jaime S. Cardoso, and Julien Cornebise, editors, *Deep Learning and Data Labeling for Medical Applications*, pages 48–57, Cham, 2016. Springer International Publishing.
- [57] Yi Zhang, Yidong Zhao, Hui Xue, Peter Kellman, Stefan Klein, and Qian Tao. Recurrent inference machine for medical image registration. *Medical Image Analysis*, 106:103748, 2025.
- [58] Shengyu Zhao, Yue Dong, Eric I-Chao Chang, and Yan Xu. Recursive cascaded networks for unsupervised medical image registration. In *Proceedings of the IEEE International Conference on Computer Vision (ICCV)*, 2019.
- [59] Shengyu Zhao, Tingfung Lau, Ji Luo, Eric I Chang, and Yan Xu. Unsupervised 3d end-to-end medical image registration with volume tweening network. *IEEE Journal of Biomedical and Health Informatics*, 2019.
- [60] Yujia Zhou, Shumao Pang, Jun Cheng, Yuhang Sun, Yi Wu, Lei Zhao, Yaqin Liu, Zhentai Lu, Wei Yang, and Qianjin Feng. Unsupervised deformable medical image registration via pyramidal residual deformation fields estimation. *CoRR*, abs/2004.07624, 2020.
- [61] Z. Zhou, B. Hong, X. Qian, et al. macnet: weakly-supervised multimodal image deformable registration using joint learning framework and multi-sampling cascaded mind. *BioMed Eng OnLine*, 22:91, 2023.
- [62] Qiaoyun Zhu, Guoye Lin, Yuhang Sun, Yi Wu, Yujia Zhou, and Qianjin Feng. Functional magnetic resonance imaging progressive deformable registration based on a cascaded convolutional neural network. *Quantitative Imaging in Medicine and Surgery*, 11(8), 2021.

- [63] Yongpei Zhu and Shi Lu. Swin-voxelmorph: A symmetric unsupervised learning model for deformable medical image registration using swin transformer. In Linwei Wang, Qi Dou, P. Thomas Fletcher, Stefanie Speidel, and Shuo Li, editors, *Medical Image Computing and Computer Assisted Intervention – MICCAI 2022*, pages 78–87, Cham, 2022. Springer Nature Switzerland.